Model biomimetic studies of templated growth and assembly of nanocrystalline FeOOH

MARIA NESTEROVA,* JOHN MOREAU,[†] and JILLIAN F. BANFIELD[†]

Department of Geology and Geophysics, University of Wisconsin-Madison, 1215 West Dayton Street, Madison, WI 53706, USA

Abstract—We studied biomimetic mineralization of self-assembling polymer matrices in order to develop a model for biomineralization of iron oxides in nature. High-resolution transmission electron microscopy (HRTEM), rheology, and fluorescence probe analyses show self-assembly of acidic polysaccharide alginic acid (Alg) to form fibrils in dilute solutions. The resulting Alg fibrils are subsequently mineralized by FeOOH in a biomimetically controlled process. Experiments were conducted in pH 9.2 solutions containing millimolar concentrations of iron at 38°C. The unperturbed state of the hybrid mineral–organic structures was studied by characterization of samples of interfacial films collected from an inorganic–organic interface. Progress of mineralization over a 4-week period was followed by HRTEM, energy-dispersive X-ray analysis, and selected area electron diffraction. Morphologies of hybrid structures determined by HRTEM, X-ray powder diffraction, Fourier transform infrared spectroscopy, energy-dispersive X-ray analysis, and selected area electron diffraction suggest formation of iron (III) oxyhydroxide phases and their assembly through a variety of mechanisms, possibly occurring simultaneously. An initial step involves precipitation of nanometer-scale amorphous particles and two-line ferrihydrite in bulk solution. Some nanoparticles assemble into chains that recrystallize to form akaganeite (β-FeOOH), presumably via a solid-state transformation pathway. Small organic molecules may mediate this process by stabilizing the akaganeite structure and controlling particle assembly. Ferrihydrite particles also bind to acidic polysaccharide fibrils and are transformed to ordered arrays of akaganeite. The parallel orientation of adjacent akaganeite nanocrystals may be inherited from the orientation of precursor ferrihydrite, possibly conferred during attachment of ferrihydrite to the polyacid fibrils. Alternatively, particle–particle interactions may induce orientation, leading to recrystallization. Subsequently, akaganeite is transformed to goethite that is characterized by nanoscale porosity and fine-scale twinning on {021}. Dislocation, twin, and nanopore microstructures are consistent with coarsening by nanoparticle assembly, possibly templated by the substrate. Nanoparticle assembly to generate biomimetic hybrid materials may be relevant to formation of complex natural biominerals in natural systems where mineral nanoparticles, small organic molecules, and more complex polymers coexist. *Copyright © 2003 Elsevier Science Ltd*

1. INTRODUCTION

Biologic activity can generate minerals with unique compositions, morphologies, and forms that may persist long after organic remains of such organic matrices associated with biomineralization are destroyed. Geomicrobiology provides many examples of composite mesostructures that are based on organic polymer molecules carrying charged functional groups along polymer chains. Model studies of mineralization on, or in proximity to, organic polymer assemblages are of direct relevance to studies of possible biosignatures (Banfield et al., 2000; Thomas-Keprta et al., 2001). Insights into morphogenesis of such materials are employed in biomimetic manufacturing of advanced materials (e.g., Davis et al., 1998; MacLachlan et al., 2000). The term "biomimetic" refers to human-made processes, substances, devices, or systems that imitate nature.

Earth science often deals with natural materials such as clays, zeolites, iron, aluminum and manganese oxides, and oxyhydroxides that constitute the inorganic component of soils, often as nanoparticles. Similarly, natural hybrid, organic–inorganic structures also contribute to the properties and health of aquatic systems. It was shown recently that a large pool of organic carbon exists in the Earth's oceans in the form of dissolved exopolymers that can undergo self-assembly (Leppard, 1995, 1997; Chin et al., 1998). For example, algae-derived organic matter provides a spectrum of various polyanions. One of them, alginic acid (Alg), consists of linear 1 to 4 linked gulurono mannuronans and is well known for its ion selectivity and tendency to form heterogeneous as well as homogeneous polymer associations (e.g., Largeau, 1995; Leppard, 1995).

An intrinsic feature of such water-soluble polyelectrolytes (PEL) is their tendency to self-assemble in, and from, aqueous solution with various counterpart species. Factors such as ionic strength, type of low- and high-molecular-weight counterions, composition of the media, and the presence of heterogeneous surfaces (charged and uncharged) all alter the geometry (conformation) of PEL molecules in the solution and the subsequent organic–inorganic composite (Dautzenberg et al., 1994). These properties enable employment of PEL in model studies of biomineralization as a process of spontaneous self-assembly.

The properties of bulk solutions containing PEL and their aggregates are nonlinear as a result of the existence of

---

* Author to whom correspondence should be addressed (masha@geology.wisc.edu).
[†] *Present address:* Department of Earth and Planetary Science, University of California-Berkeley, Berkeley CA 94720, USA

charged domains along the polymer chains. As a result of strong, predominantly ionic and hydrophobic interactions, alginates are known in nature as "scavengers" of various counterparts in solutions (e.g., dyes, hydrocarbons, metal hydrolyzed species, other macromolecules). The templating function of such polymers in the formation of organic–inorganic composites has been noted previously (Williams, 1984; Mann, 1993; Heywood, 1996; Ozin et al., 1997; Jones et al., 2000; Nesterova et al., 2000).

A number of recent studies of Fe(III)-polymer matrix biomimetic mineralization have reported the influence of the organic matrix structure on the mineral phase nucleation and crystallization processes, mostly at elevated temperatures and pHs between 10.3 and 13. Generally, preformed functional matrix templates were employed (Kroll and Winnik, 1996; Breulmann and Colfen, 1998; Dante et al., 1999; Dutta et al., 2000; Jones et al., 2000). The objective of the present study was to devise a model mineralization system that permits *simultaneous* formation of a templating polymer matrix through self-assembly and its controlled *biomimetic* mineralization by iron (III)-containing hydrolyzed species at millimolar concentration of iron(III) and pH of natural aquatic systems.

In the range $5 < pH < 9$, which is pertinent to biologic and aquatic systems, hydrated transition metal species pervading the aqueous pools need to be stable for long enough to function in biomineralization. This is achieved mainly through formation of mixed metal–organic complexes (Schneider and Erni, 1985; Wu et al., 2001). In the biomimetic studies reported here, tris(acetylacetonato) Fe(III), $(Fe(acac)_3)$ (or 2,4-pentanedione Fe(III)) was chosen as a the starting iron-containing compound because it forms comparatively stable, polynuclear hydrolyzed species at neutral and basic conditions; thus, it can serve as the transit pool species in biomimetic mineralization (Echmaeva et al., 1994).

In our experiments, special consideration was given to handling of fragile and colloidal structures to prevent damage to their architecture. Our strategy was to introduce an additional interface—that is, to create a boundary area between aqueous and organic phases that enables formation of hybrid, organic–inorganic structures. From this interfacial area, the samples could be collected for characterization by transmission electron microscopy (TEM). The interface has characteristics that make it an important proxy for natural processes because biomineralization often occurs at boundaries between more hydrophilic (aqueous) and more hydrophobic (colloidal particle, micelle, solid surface) regions (MacLachlan et al., 2000).

2. MATERIALS AND METHODS

Alg, sodium salt (Sigma-Aldrich; from *Macrocystis pyrifera*[kelp], high viscosity) was used. The carboxylic group content, determined by colloid titration with chitosan, was 18.3% (theoretical, 22.3%). Borate (pH 9.2) buffer solution was prepared from commercial tablets (BDH & Merck Laboratory Chemicals). Iron(III) acetylacetonate $(Fe(acac)_3)$, 99% purity (Aldrich Chemical) was used. The fluorescence probe, *N,N*-dymethyl-1-naphthylamine (DMNA), was obtained from Sigma. Pyrocatechol violet (pyrocatechol sulfonphtalein) and crystal violet dyes were purchased from Fisher.

A total of 100 mL of freshly prepared dilute pH 9.2 buffer solution containing 0.05 g (1.396×10^{-3} mol/L) of $Fe(acac)_3$ and 0.0119 g of Alg was placed into each of six 250-mL flasks. The amount of polyacid

was calculated to provide Fe: $COO^- = 3:1$ (Nesterova et al., 2000). To localize formation of the organic–inorganic composite phase, hexane (100 mL) was carefully added to each flask to generate an upper organic layer immiscible with the aqueous solution. Sealed flasks were placed in a shaker and thermostated at 38°C for 6 weeks.

Control iron-free solutions were prepared, and the geometry of interfacial iron-free polymer films was studied after 4 weeks of incubation at 38°C. For visualization, $\sim 5 \times 10^{-6}$ mol/L pyrocatechol violet was added to the aqueous polymer solution layers that did not contain iron (III) compounds before the 4-week incubation.

In some experiments (e.g., for polymer fibril morphology studies), no iron (III) or pyrocatechol violet dye was used. Instead, interfacial polymer films were stained with crystal violet after 4 weeks of incubation at 38°C. Films were characterized by light microscopy with a Leica Leitz DMR microscope.

During the hydrolysis, stable thin films separating the organic and aqueous phases and containing solid aggregates were sampled periodically (after 4, 10, and 18 d, 4 weeks, and 6 weeks), mounted on Formvar-coated grids, and coated with carbon for examination by high-resolution transmission electron microscopy (HRTEM).

When the hydrolysis was completed, precipitates formed in all flasks were collected, washed three times with water and once with absolute ethanol, and dried by lyophilization. These samples were characterized by X-ray powder diffraction (XRD), Fourier transform infrared spectroscopy (FTIR), and HRTEM. XRD used a Scintag automated powder diffractometer operated at 35 kV and 40 mA with the Cu-Kα radiation tube. TEM-based studies were carried out with a Philips CM200UT TEM with a 0.2-nm point resolution operated at 200 kV. Compositional microanalyses were collected via TEM-based energy-dispersive X-ray spectrometry. FTIR data were collected with a Nicolet 740 FTIR spectrometer. Mineralized, unmineralized, and stained films were examined with a light microscope.

To elucidate the process of polymer matrix self-assembly, the rheology of Alg solutions was studied by viscometry and surface tension measurements. Fluorescence probe studies were employed to determine the conformational state of the polyacid. A Cannon-Ubellohde glass capillary viscometer (Cole-Parmer Instruments) with a flow time for water of 180.87 ± 0.5 s at 25°C was used. Surface tension was measured by a platinum ring method with a du Nouy tensiometer calibrated to provide direct values of γ, the surface tension coefficient (N/m^2). At least three measurements were made for each solution. The data obtained were reproducible, with negligible deviation.

To test hydrophobic properties of microdomains created by polyacid molecules (and their associates) in bulk solution, fluorescence probing by DMNA was carried out as follows: aliquots of Alg solution containing a calculated amount of polyacid and solution of DMNA were quickly mixed in a volumetric flask, the volume adjusted, and emittance spectra recorded on a Perkin-Elmer MPF-66 spectrometer at room temperature. All measurements were carried out with isoionic dilution.

3. RESULTS

During 6 weeks of hydrolysis of $Fe(acac)_3$ solutions, the thin films separating organic (hexane) and inorganic (aqueous) layers in the flasks developed mineralized composite material that contained submicron particles of hydrolyzed iron(III) compounds. Polymer interfacial films also formed in iron-free solutions.

3.1. Examination of Polyacid Phase

Figure 1 shows light microscope and TEM images of interfacial polyacid films collected from the organic–inorganic interface in iron-free solutions. Light microscope images demonstrate straplike, 1 to 5 μm wide, hundreds of micron long polymer fibrils that are mutually aligned (Fig. 1a). TEM images reveal the detailed structure of polymer
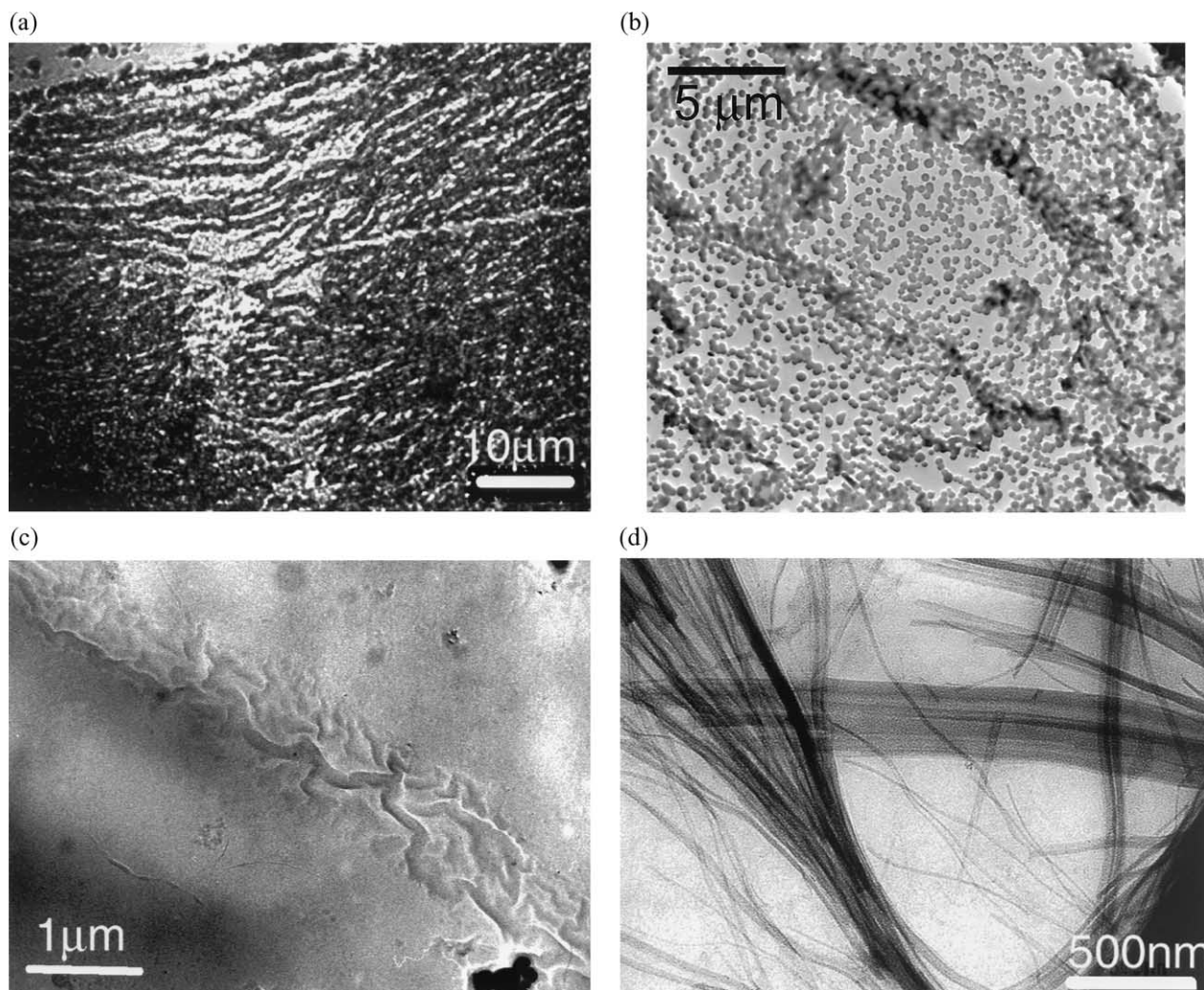
(a)

(b)

(c)

(d)

Fig. 1. Images of self-assembling Alg fibrils in an unperturbed state as collected in an interfacial organic-aqueous layer: (a) field of polyacid fibrils aligned (light microscopy), (b) TEM picture of separate polymer fibrils visualized by sorption of hydrophobic dye particles, (c) single braided polymer fibril of complex morphology, and (d) thin threads and "sheets" of Alg filaments (Crystal Violet stain).

arrangements as visualized by sorption of electron dense particles of dye. Twisted and braided single polymer fibrils are ~1 μm wide (Figs. 1b,c). A TEM image of a specimen of interfacial polyacid film formed in the absence of interacting counterparts in the solutions, and stained with crystal violet after its formation, is shown in Figure 1d. Long, thin filaments of polyacid, visualized by sorption of electron-dense dye species, resemble the extracellular polymer phase observed in slimy microalgae materials (Leppard, 1997). Some filaments self-assemble and form thin polymer ribbons (Fig. 1d).

To study the conformational state of Alg molecules, viscometry, surface tension, and fluorescence probe studies were carried out in the dilute polymer solution at low (I = 3.7×10^{-2} mol/kg; [Na$^+$] = 2.7×10^{-2} mol/L, [Cl$^-$] = 6.9×10^{-3} mol/L, [B$_2$O$_7$$^{-2}$] = 10^{-2} mol/L) and very low ionic strength

(ultrapure water, conductivity 5.5 μS/m). Flexible polyelectrolyte molecules such as dissociated Alg usually possess a rodlike expanded conformation state in dilute, low-ionic-strength solutions as a result of the electroviscous effect (Molyneux, 1983). The value of solution viscosity number, η, relates to the hydrodynamic volume of a single polymer molecule in the solution. The data obtained from viscosity and surface tension measurements of dilute Alg solutions in pure water are presented in Figure 2.

The plot of Alg solution viscosity number η vs. polymer concentration C (Fig. 2, plot a), shows a clear maximum at polyacid concentration near 1×10^{-4} g/mL. In the same concentration region, the broad minimum of γ, surface tension coefficient values can be observed, as shown in Figure 2, plot b. These changes in solution properties at Alg concentrations ~1×10^{-4} g/mL presumably correspond to the expanded
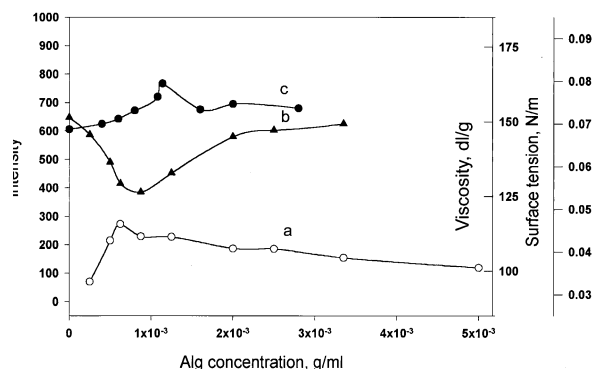
Fig. 2. Changes of reduced viscosity (η_{red}), surface tension (γ), and fluorescence intensity of Alg solutions (c) as a function of polymer concentration, C.

Fig. 3. Effect of Alg on fluorescence emission spectra of DMNA in aqueous solution at pH 9.2. Solution contains 9.2×10^{-4} mol/L of DMNA and (from top to bottom) 1.08×10^{-4}, 1.14×10^{-4}, 6×10^{-5}, none, 2×10^{-4}, 8×10^{-5}, 2.8×10^{-4}, 3.6×10^{-5}, and 2×10^{-5} g/mL of polyacid in dilute pH 9.2 buffer. Inset shows relation between fluorescence intensity of DMNA probe at 441 nm and concentration of polymer in μQ water and dilute pH 9.2 buffer.

conformation of Alg molecules in the solutions, conditions close to those of our experiments. We propose that the surface tension minimum relates to the conformational state where the expanded polyacid molecules (or their aggregates) form a surface layer, with their hydrophilic carboxylic groups facing the bulk aqueous solution.

DMNA was used as a fluorescence probe to investigate local environments within the polymer self-assemblies. In general, DMNA fluorescence intensity increases, or the fluorescence maximum of DMNA spectra shift toward the shorter wavelengths upon increasing hydrophobicity of the probe's surroundings (spectral blue shift) (Ohtaki, 1998). Figure 3 shows the effect on the DMNA emission spectra of change in polyacid concentration with constant fluorescence probe concentration in very dilute pH 9.2 buffer solution. A similar but more pronounced effect was obtained for solutions prepared with pure water (data not shown). This is due to withdrawal of the shield effect of small ions, which is followed by unfolding of polyacid molecules to a more expanded state. The solution compositions are described in the caption. The fluorescence intensities in low concentration pH 9.2 buffer and in pure water were also recorded at the 441-nm maximum. The data obtained are shown in the inset in Figure 3. The plots demonstrate a steep increase in fluorescence in tensity of the DMNA probe at an Alg concentration of $\sim 1 \times 10^{-4}$ g/mL for both solutions sets, close to the polyacid concentration used in our experiments (1.119×10^{-4} g/mL). The presence of hydrophobic interacting surfaces capable of hosting the hydrophobic particles of DMNA is inferred in the polyacid chains at these conditions. Although spectroscopic data show reproducible changes in fluorescence intensity with change in polyacid concentration, no reproducible blue shift in spectra was observed during any measurements.

Comparing the fluorescence intensity of the DMNA probe at the 441-nm maximum in the μQ water solution (Fig. 3 inset as plot 1; also presented as plot c in Fig. 2) and Alg solution rheology data (Fig. 2, we observed that the sharp maximum in fluorescence intensity of DMNA in polyacid solutions occurs in the polymer concentration region limited by dashed lines and
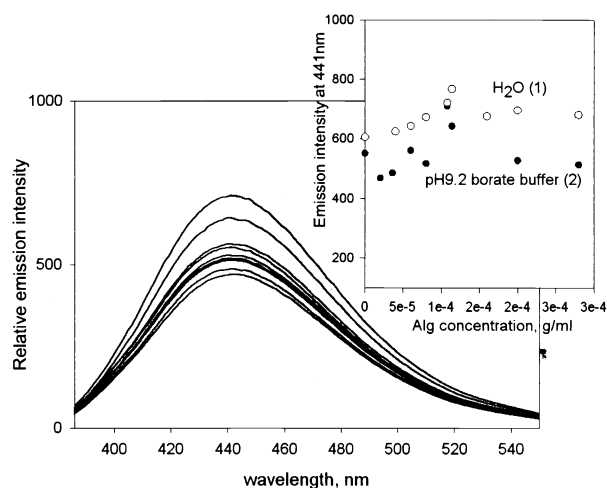
related presumably to most expanded conformation of Alg molecules. Thus, the data of all three methods—viscometry, fluorescence probe analysis, and surface tension measurements—are in agreement.

3.2. Examination of Inorganic–Organic Composite Phase

Amorphous, crystalline, and hybrid organic–inorganic structures coexist in the interfacial polymer films. HRTEM images and energy-dispersive X-ray analysis analyses of particles from interfacial films collected after 4 to 10 d generally indicate amorphous aggregates of iron oxyhydroxide compounds (data not shown). HRTEM images of Alg-containing interfacial films that hosted growth of iron(III)-containing solid phases are shown in Figure 4. In some cases, samples of Alg fibrils collected after 10 to 14 d were covered by mineral particles of <2 nm diameter (Fig. 4a).

Images of specimens of organic–inorganic interfacial films prepared after 2 to 4 weeks of mineralization are shown in Figures 4b −e. Submicron-wide fibrils of Alg are encrusted with large (> 50 nm wide) iron oxyhydroxide crystals (see inset). The ~1-nm periodicities are consistent with identification as goethite or akaganeite. The presence of these large platy crystals suggests that growth was templated by the polymer matrix.

Figure 4c shows fibril assemblies that host many needle-like nanocrystals, as shown in the inset. Crystals with average lengths of 10 to 30 nm, and aspect ratios of ~9.2 proved to be unstable under the electron beam. However, ~0.29-, 0.52-, 0.65-, and 0.7-nm lattice fringes were detected in these mineral particles, consistent with their identification as
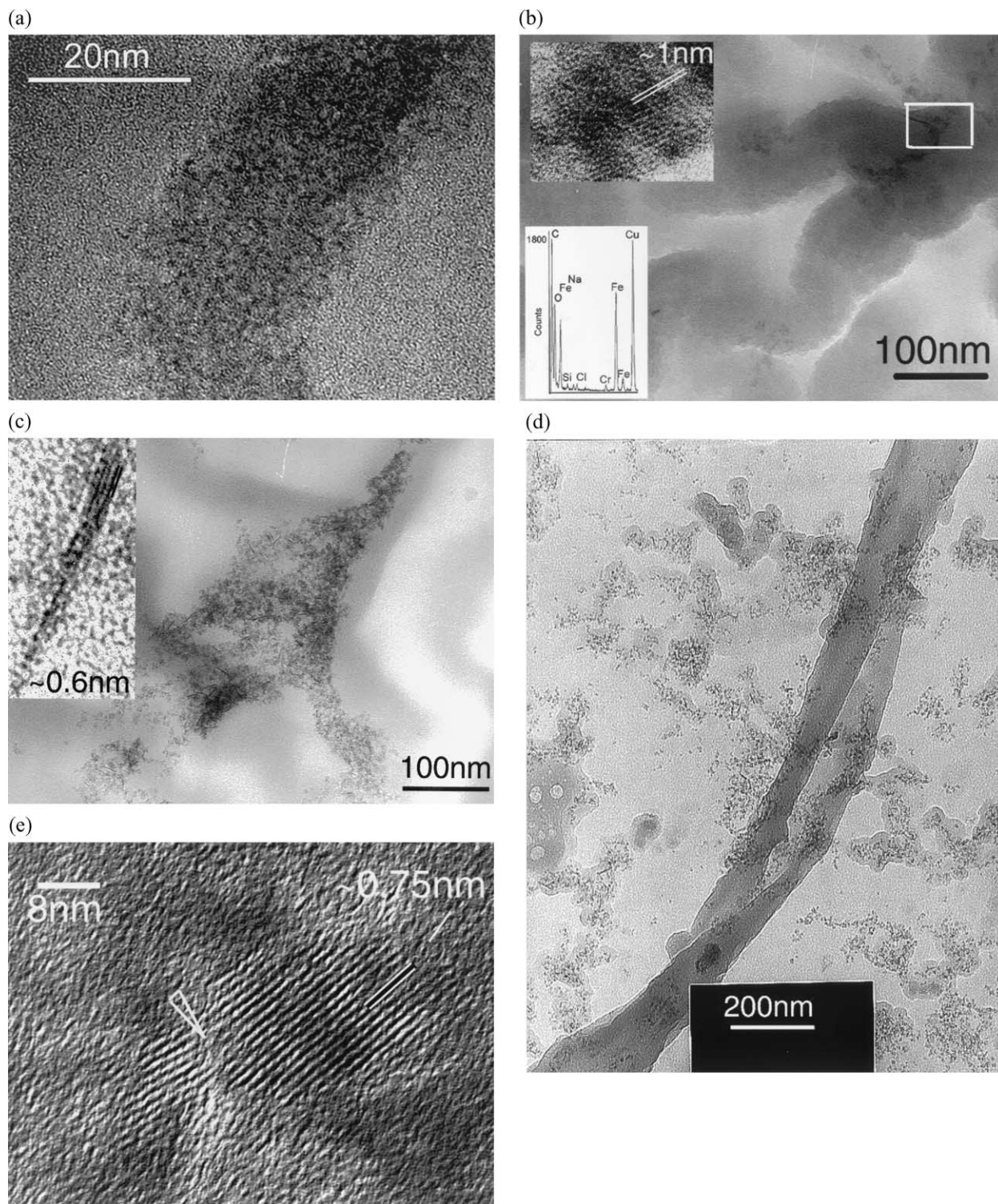
Fig. 4. HRTEM images of representative morphologies of polyacid fibrils that template mineralization of iron(III) oxohydroxy phase: (a) a single fibril covered with ∼ 2-nm-diameter iron oxyhydroxide particles at early stages of mineralization; (b) Alg fibrils "encrusted" with FeOOH phase with 1-nm lattice fringes; (c) fibrils that host a mesocrystalline FeOOH phase consisting of needlelike crystals; (d) polymer ribbonlike assembly visualized by sorption of electron dense species from mineralization solution; and (e) area of Alg fibril-template mineralized by two platy particles.

akaganeite (β-FeOOH). Some needlelike akaganeite appear to be constructed from chains of nanoparticles. The crystals follow the geometry of the fibrils in these unperturbed hybrid assemblies, indicating templation by the polymer matrix.

In Figure 4d, the geometry of a single, ribbonlike Alg assembly is visualized by sorption of electron dense species (probably iron) from the mineralization solution. Figure 4e shows a segment of the surface of a mineralized single fibril where two platy mineral particles are semialigned. An edge dislocation is associated with the low angle grain boundary between the nanocrystals. The d-values calculated from lattice fringes observed in various crystalline areas on the surface of this submicron fibril by HRTEM, are 0.75 nm (shown in Fig. 4e), 0.34 and 0.52 nm (data not shown). The set of d-values for these fringes is closest to that of akaganeite.

The experimental study of the interfacial growth of iron(III) oxyhydroxide aggregates yielded specimens after 4 weeks of hydrolysis that contain micron-scale acicular crystals as shown in Figure 5a., associated with organic–inorganic interfacial films containing needlelike crystals (as shown in the inset). Electron diffraction studies confirmed that these are goethites that consist of multiple smaller rodlike crystals that are mutually aligned to generate the typical lathlike goethite crystal form. At higher magnification, the fine structure of the crystals can be observed (Figs. 5b–d). Nanoscale domains separated by porosity indicate that the large goethite laths are composed of aligned nanocrystals with an average diameter of 5 to 8 nm. These are crystallographically "docked" to form a fairly smooth solid surface (Fig. 5b). Lattice fringes with d-spacing values of approximately 0.4 nm ({101} goethite) indicate that nanoparticles are either crystallographically oriented with respect to each other or are oriented so that adjacent nanoparticles are in twin-related orientations with twin planes on {021} (Cornell, 1996). The two orientational relationships occur with about equal probability.

Figure 5c depicts part of an acicular crystal of goethite. The {101} lattice fringes indicate that nanocrystals in this region are imperfectly oriented with respect to each other (misorientation indicated by rotation of lattice fringes are marked). Figure 5d displays a region of the goethite aggregate shown in Figure 5a viewed down [−111]. Roughly hexagonal-shaped domains of low diffraction contrast indicate thin regions of separate islands of goethite (note the {101} (0.42-nm spacing) and {110} (0.28-nm spacing) lattice fringes). On the basis of the HRTEM results, we infer that these biomimetic materials are constructed from aggregates of epitaxially attached FeOOH nanocrystals, similar to observed recently in natural materials and aged colloids (Alivisatos, 2000; Penn et al., 2001).

To compare templated (interfacial) and nontemplated mineral phases formed in bulk solution, specimens of the bulk precipitate from mineralization solutions were characterized by HRTEM, XRD, and FTIR. XRD and HRTEM data show that most of the bulk precipitate is poorly ordered, yet it contains occasional crystals that range in size from micron to nanometer scale. Electron diffraction studies yielded sets

of d-values consistent with ferrihydrite (0.25, 0.198, 0.147 nm) and akaganeite (0.56, 0.528, 0.27, 0.217, 0.184 nm). Nanoscale needlelike particles identified as β-FeOOH (e.g., inset in Fig. 5a) were found both in precipitates formed in bulk solution and interfacial hybrid films (e.g., Fig. 4c). The formation and stabilization of nanoparticles of akaganeite (β-FeOOH) (possible primary products of hydrolysis) we attribute to the presence in solution of large anions (such as acetylacetonate and, possibly, borate) and also Cl^- (Schneider and Erni, 1985; Reeves and Mann, 1991; Schwertmann et al., 1996; Saric et al., 1998; Music et al., 1999; Deliyanni et al., 2001).

In some cases, aggregates formed in bulk solution are flocculated with polymer fibrils (Fig. 6). An FTIR spectrum confirmed the presence of significant organic material in the bulk precipitate. This is likely to be sorbed acetylacetonate ligand and the polyacid phase (two strong peaks observed at 1618 cm^{-1} and 1400 cm^{-1} were attributed to C=O groups vibration and stretching). A broad shoulder in the spectrum at 490 to 400 cm^{-1} was attributed to Fe-O interactions. The particulates formed in bulk solution (Fig. 6) are generally similar to those found in aquatic natural systems and observed in recent studies of mineralization of polysaccharide matrices (Leppard, 1995; Chin, 1998). The major difference between the bulk precipitate and the interfacial mineral phase lies in the very small size of interfacial film mineral aggregates and the practical absence in the bulk precipitate of micron-sized acicular goethites, as shown in Figure 6.

4. DISCUSSION

In solution, polar molecules of Alg dissociated at pH 9.2 bear functional groups that confer water solubility and dispensability to the polymer. At the hydrocarbon–water boundary (or the air–water boundary), the molecules are positioned so that the generally more hydrophobic carbohydrate backbones face a more hydrophobic phase. Thus, the carboxylic functional groups of the surface polymer molecules are pointing inward to the water phase, forming a thin two-dimensional functional surface film that serves as a template for mineralization. In very dilute solutions with very low ionic strength, some strong polyanions such as Alg acquire an expanded, rodlike conformation of chains that is manifested in negative slope of the viscosity number (η) vs. polymer concentration (c) plot (plot 1, Fig. 2; area limited by dashed lines). The reverse of the slope after maximum η in the more dilute region has been attributed to intermacromolecular interactions, presumably governing the solution properties even in this very dilute region (Dautzenberg et al., 1994).

Molecular modeling investigations reported recently predict that both α-L-polyguluronic (G-block of Alg, rigid chain) and β-D-polymannuronic (M-block, semirigid chain) polysaccharide residues exist as right-handed helices with a twofold screw periodicity; the β-D-polymannuronic chain can also form a threefold helix (Braccini et al., 1999). Acidic polysaccharide chains in the solution are considered to be highly hydrophilic as a result of the large number of polar functional groups. Nevertheless, recent studies provide ex-
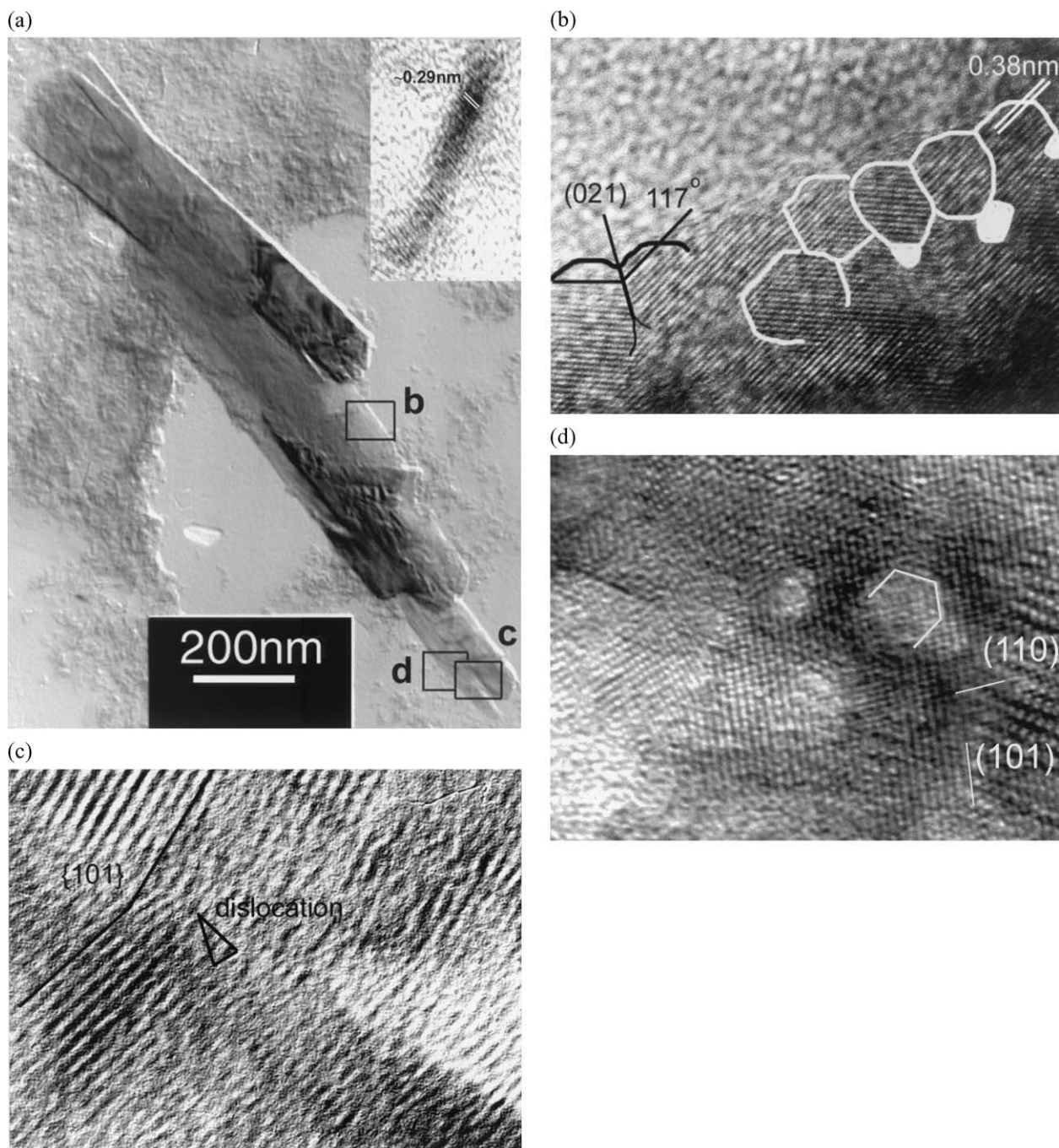
Fig. 5. HRTEM image of typical aggregate of acicular goethites crystals from a composite interfacial film: (a) small rotational misalignments between oriented acicular crystals; inset shows needlelike akaganeite crystal found in the area; (b) oriented attachment of nanoscale crystallites (area (b) of picture (a)); (c) low angle rotational misorientation between two acicular almost parallel goethites (area (c) of picture (a)); and (d) porosity incorporated into goethite crystalline region ((d) area of picture(a)); note the hexagonal shape of incorporated pores.

perimental and theoretical evidence that some polysaccharide conformations demonstrate amphiphilic properties in solution as a result of the spatial geometry of their polymer units. It appears generally that polysaccharides that adopt

the helix-structure might be amphiphilic (Balasubramanian, 1993). In our studies, the DMNA fluorescence probe experiments provide evidence for the possible presence of hydrophobic binding sites or environments in expanded Alg mol-
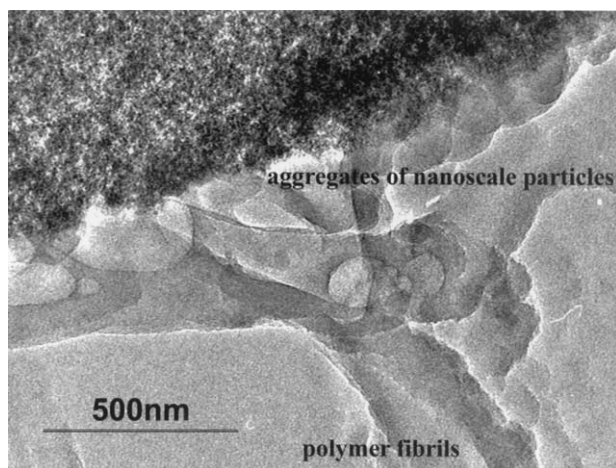
Fig. 6. Typical composite flocculate from bulk solution containing aggregates of iron(III) oxyhydroxide nanoparticles (two-line ferrihydrite) and polymer fibrils.

ecules in aqueous solution of low ionic strength at high dilution. We presume that this is followed by thermodynamically driven self-assembly of polymer chains and their aggregates as a result of the persistent energy-minimized conformation of molecules in the solution. This is consistent with atomic force microscopy (AFM) data from very dilute alginate solutions (Decho, 1999).

In the absence of counterparts in the solution that promote polymer aggregation as shown in Figures 1a,b, Alg fibrils driven to the aqueous–organic interface exhibit a rather filament-like morphology (Fig. 1d). Introduction of "binding" moieties such as hydrolyzed transition metal species and voluminous hydrophobic dye particles resulted in a distinctive, straplike structure of the composite aggregates (Fig. 1a–c). Sorption on polyanion fibrils of pyrocatechol violet and the metachromatic color change of the solution from yellow to green due to aggregation and stabilization of dye species suggest possible Van der Waals and hydrophobic interactions between polymer fibrils and the dye species. Additionally, specific Alg-Fe(III) binding is considered to occur in solutions containing hydrolyzing iron-containing polynuclear species (Leppard, 1995; Jones et al., 2000; Nesterova et al., 2000). We propose associative polymer network formation that is based on helix–helix polysaccharide aggregation that is thermodynamically driven and promoted by binding of counterparts such as the metal ions or the organic dyes. Eventually, this leads to higher levels of lateral ordering of the system and results in phase separation, as exemplified by light and electron microscopy results reported here.

Formation and growth of biomimetic polyacid fibrils (flocs) results both from the continuous assembly of free expanded Alg molecules and from secondary aggregation and dewatering of small assembled strands. This drives them to the hydrophilic-hydrophobic interface. In our experiments, we have also observed that polymer fibrils can further aggregate on the interface and mutually align to form "fields." The resulting

two-dimensional self-assembled organic matrix controls biomimetic mineralization of iron (III) species, determines the orientation of templated crystal growth, acts as a substrate for assembly of nanoparticles, or some combination of these. Although polyanion molecules that are flexible in solution may act as crystal growth inhibitors, the same macromolecules can act as nucleators when immobilized on a stable surface or self-organized to provide such surface. Then they facilitate the steady unperturbed growth of the crystals (Heywood et al., 1988; Reeves and Mann, 1991; Furedi-Milhofer and Sarig, 1996). The alginate fibrils employed in our experiments may have played both roles: inducing specific growth of platelets on the fibrils and inhibiting crystallization of amorphous materials in bulk solution.

The Ostwald rule of stages (Nyvlt, 1995) predicts that in solutions, the first formed solid will be a metastable hydrolyzed iron (III)-containing compound. Subsequently, the other thermodynamically stable phase crystallizes, either directly or after transformations involving other metastable polymorphs. In our experiments, the first-formed solid often consists of aggregates of <2-nm particles (Fig. 5). Some of the nanoparticles are amorphous; others have a structure related to two-line ferrihydrite or feroxyhite (Flynn, 1984).

Combining available data, we infer that the mineralization solution contains colloidal multinuclear clusters as well as the above-mentioned ~2-nm-diameter nanoparticles (Flynn, 1984; Gregory and Duan, 2001). The particles may aggregate in solution and subsequently adhere to polymer fibrils. Alternatively, the aggregation may take place at least in part on the fibril surface. In the latter case, the fibrils could serve to stabilize potentially unstable nuclei. This is essentially a heterogeneous nucleation process wherein the organic functional groups bind to ions on the cluster or nanoparticle surface, reducing the surface energy and thus the tendency of the particles to dissolve. Thus, the alginate polymer is a substrate for mineral crystallization.

Recent studies indicate that the presence of an organic–inorganic interface in hydrolytic iron (III)-containing solution can lead to crystallization of β-FeOOH (Reeves and Mann, 1991; Coe et al., 1995; Dante et al., 1999; Kilcoyne and Lawrence, 1999; Gossuin et al., 2001; Wirnsberger et al., 2001). After 4 weeks of hydrolysis and mineralization, Alg fibrils in our experiments were encrusted with akaganeite (β-FeOOH) (Fig. 4e). Formation of this phase, which is normally regarded as thermodynamically unstable at pH 9.2, could be attributed to the presence of the charged acidic functional surface of the polyacid fibrils or acetylacetonate anions in aggregates in bulk solution. The polymers may alter the kinetics of nucleation and the transformation of the iron oxyhydroxide phase and delay the progress of mineral particle growth (Williams, 1984; Kurimura, 1991; Furedi-Milhofer and Sarig, 1996; Heywood, 1996). Alternatively, akaganeite may be the thermodynamically stable phase because its surface energy is reduced significantly as a result of surface-bound organics ligands. It is also possible that akaganeite has a lower surface energy than other FeOOH structures and becomes the stable phase as a result of a size-related thermodynamic phase stability reversal (Gribb and

Banfield, 1997; McHale et al., 1997; Zhang and Banfield, 1998).

It is intriguing that akaganeite is only observed as small crystals and goethite occurs only as larger crystals in our samples. If surface energy contributes to phase stability and influences the precipitate structure in this system, then phase transformation of akaganeite induced by crystal growth is expected. The nanoscale twinning in goethite (Fig. 6) may be a transformation microstructure that arises from random nucleation of the goethite product in one of two symmetrically (twin)-related orientations. Existence of a transformation twinning would imply that the goethite forms from akaganeite by an essentially solid-state transformation pathway. Alternatively, the microstructure could be generated by oriented aggregation based growth involving goethite nanoparticles (Penn and Banfield, 1998a, b).

Recent work suggests that the typical particle size of the organically bound iron(III) oxyhydroxide phase is determined by the "capacity" of templating surface—that is, a continuous functional organic phase may template a continuous solid phase, both in synthetic biomemetic products (Dautzenberg et al., 1994; Coe et al., 1995; Wirnsberger et al., 2001) and natural materials (Banfield et al., 2000). In contrast, mesoscopic akaganeite needles observed in our specimens form on functional interfaces that provide restricted area for nucleation such as aggregates of acetylacetonate amphiphilic moieties (Reeves and Mann, 1991; McHale et al., 1997; Dante et al., 1999). This explains the formation of akaganeite nanoscale needles both in bulk solution and in interfacial organic films in our experiments.

The multigrain, particulate nature of iron oxohydroxy aggregates was observed in many composite film specimens, as depicted, for example, in Figure 4a, e.. Such crystal morphology may originate from the presence in the templating matrix of multiple, closely situated nucleation centers. These enable nucleation of primary particles and further growth of minerals by oriented attachment of nanoscale precursors (Banfield et al., 2000) followed by coarsening.

Prior nanoparticle studies have focused on aggregation-based growth in two contexts. First, supercrystal arrays consisting of oriented, isolated nanoparticles bound into a periodic array by organics can be formed (Murray et al., 2000). In this case, upon removal of organic matter separating the nanoparticles, crystal growth could yield large single crystals. Secondly, nanocrystals can aggregate on the organic substrate. If crystals are free to rotate, then growth can occur when surfaces are eliminated by formation of coherent interfaces (Penn and Banfield, 1998a, b).

Defect microstructures characterize materials in which crystal growth proceeds via an aggregation-based mechanism. Lattice fringe images of materials formed in this study provide evidence of line, planar, and three-dimensional defects associated with nanocrystal interfaces. Specifically, we observed multiple dislocations, as shown in Figures 4c and 5b–d, twins, and nanometer-scale pores evidenced by zones of low contrast (Fig. 5d). These may indicate growth by an aggregation-based pathway. However, if two particles are semioriented with respect to each other, then dislocations will be present at the interface, regardless of the reason why the particles are misoriented. In this study, misorientation may be due to imperfect substrate templation of growth or restricted rotational movement of primary particles after docking onto polymer substrate. Pores may form for a variety of reasons (e.g., organic inclusions, mineral particles misalignment) and could be preserved because of the low solubility of iron-containing phase and slow diffusion rates.

Biomimetic mineralization of the Alg matrix leads to formation of porous acicular goethites. These acicular crystals occur in aggregates in which the goethite crystals are crystallographically oriented or are related by small rotations, as shown in Figure 5a. The acicular crystals themselves appear to be constructed from oriented nanoparticles that may have assembled before transformation to goethite. Thus, biomineralization of the alginate polymer appears to involve oriented assembly of FeOOH building blocks over a large range of scales.

The biomimetic process observed in our experiments may be related to the process of formation of similar acicular goethite in natural microbial mats (e.g., Konhauser and Ferris, 1996; Akai et al., 1999). Acicular goethites also occur in extracellular matrices associated with some bacteria, where their formation is attributed to both metabolic bacterial activity and nonspecific sorption by polyacidic extracellular polymers that are commonly associated with bacteria. Similar goethites are found commonly in other living matter connected with templated processes of iron biomineralization, such as in hemosiderin, where close association of the organic components with the nanoscale iron particles is present (Chua-anusorn and Webb, 2000).

Spontaneous formation of Alg fibrils and their subsequent mineralization by iron(III) oxyhydroxide, as shown in Figure 4, may be related to a natural process suggested recently for the formation of organic fibrils due to aggregation of the oceanic dissolved organic matter (Leppard, 1995, 1997; Chin et al., 1998). The latter is often triggered by organic pollutants (i.e., hydrophobic substances) that promote phase separation. As in natural decontamination of water bodies, aggregation may start with binding of metal species or organic contaminants such as petroleum products by polymers or polymer aggregates.

The presence of akaganeite in nature, mostly in aquatic systems, has been attributed previously to the salinity of seawater—that is, to the presence of Cl^- that is included in the crystal structure of akaganeite (Eggleton et al., 1988; Schwertmann et al., 1998). Our results suggest that organic matter may play a key role in inducing akaganeite crystallization during biomineralization of cell-associated polymers, or when an organic matrix is available in bulk solution, both in form of high-molecular-weight compounds (and their aggregates) and associates of amphiphilic organic molecules of low molecular weight.

Associate editor: P. A. Maurice

REFERENCES

Akai J., Akai K., Nakano S., Maki Y., and Sasagawa I. (1999) Biologically induced iron ore at Gunma iron mine, Japan. *Am. Mineral.* **84,** 171–182.

Alivisatos A. P. (2000) Biomineralization—Naturally aligned nanocrystals. *Science* **289,** 736–737.

Balasubramanian D., Raman B., and Sundary C. S. (1993) Polysaccharides as amphiphiles. *J. Am. Chem. Soc.* **115,** 74–77.

Banfield J. F., Welch S. A., Zhang H., Thomsen Ebert T., and Lee Penn R. (2000) Aggregation-based crystal growth and microstructure development in natural iron oxyhydroxide biomineralization products. *Science* **298,** 751–759.

Braccini I., Grasso R. P., and Perez S. (1999) Conformational and configurational features of acidic polysaccharides and their interactions with calcium ions: A molecular modeling investigation. *Carbohydrate Res.* **317,** 119–130.

Breulmann M. and Colfen H. (1998) Elastic magnets: Template-controlled mineralization of iron oxide colloids in a sponge-like gel matrix. *Adv. Mater.* **10,** 237–241.

Chin W.-C., Orellana M. V., and Verdugo P. (1998) Spontaneous assembly of marine dissolved organic matter into polymer gels. *Nature* **391,** 568–572.

Chua-anusorn W. and Webb J. M. J. (2000) The effect of prolonged iron loading on the chemical form of iron oxide deposits. *Inorg. Biochem.* **79,** 191–200.

Coe E. M., Bereman R. D., and Monte W. T. (1995) An investigation into the size of an iron dextran complex. *J. Inorg. Biochem.* **60,** 149–153.

Cornell R. M. and Schwertmann U. (1996) The Iron Oxides: Structure, Properties, Reactions, Occurrence and Uses. Pp 167, Weinham; New York: VCH.

Dante S., Hou Zh., Risbud S, and Stroeve P. (1999) Nucleation of iron oxy-hydroxide nanoparticles by layer-by-layer polyionic assemblies. *Langmuir* **15,** 2176–2182.

Dautzenberg H., Jaeger W., Kotz J., Philipp B., Seidel C., Stscherbina D. (1994) Characterization of macromolecular parameters in polyelectrolyte solutions. In *Polyelectrolytes: Formation Characterization and Application* (ed. H. Dautzenberg et al.), pp. 182–220. Carl Hanser Verlag.

Davis S., Patel H., and Mann S. (1998) Brittle bacteria: A biomimetic approach to the formation of fibrous composite materials. *Chem. Mater.* **10,** 2516–2524.

Decho A. (1999) Imaging an alginate polymer gel matrix using atomic force microscopy. *Carbohydrate Res.* **315,** 330–333.

Deliyanni E. A., Bakoyannakis D. N., Zouboulis A. I., Matis K. A., and Nalbandian L. (2001) Akaganeite-type beta-FeO(OH) nanocrystals: Preparation and characterization. *Microporous Mesoporous Mater.* **42,** 49–57.

Dutta A., Jarero G., Zhang L., and Stroeve P. (2000) In-situ nucleation and growth of gamma-FeOOH nanocrystallites in polymeric supramolecular assemblies *Chem. Mater.* **12,** 176–181.

Echmaeva T., Khramov A. V., and Berdnikov V. M. (1994) Nature of active forms of trivalent iron–induced luminolol oxidation. *Zh. Fiz. Khimii* **68,** 1563–1567.

Eggleton R. A., Schulze D. G., and StuckiJ. W. (1988) Introduction to crystal structures of iron-containing minerals. In *Iron in Soils and Clay Minerals.* NATO ASI Series, Series C: Mathematical and Physical Sciences, Vol. 217 (eds. J. W. Stucki et al.), p. 161. Reidel.

Flynn C. M. (1984) Iron (III) hydrolysis. *Chem. Rev.* **84,** 31–63.

Furedi-Milhofer H. and Sarig S. (1996) Interaction between polyelectrolytes and sparingly soluble salts. *Prog. Crystal Growth Charact.* **32,** 45–75.

Gossuin Y., Roch A., Lo Bue F., et al. (2001) Nuclear magnetic relaxation dispersion of ferritin and ferritin-like magnetic particle solutions: A pH-effect study. *Magnet. Reson. Med.* **46,** 476–481.

Gregory J. and Duan J. M. (2001) Hydrolyzing metal salts as coagulants. *Pure Appl. Chem.* **73,** 2017–2026.

Gribb A. A. and Banfield J. F. (1997) Particle size effects on transformation kinetics and phase stability in nanocrystalline TiO$_2$. *Am. Mineral.* **82,** 717–728.

Heywood B. R. (1996) Template-directed nucleation and growth of inorganic materials. In *Biomimetic Materials Chemistry* (ed. S. Mann), pp. 143–152. VCH.

Heywood B. R., Rajam S. R., Bircall J. D., et al. (1988) Crystallochemical recognition at organized inorganic–organic interface. *J. Biochem. Soc. Trans.* **16,** 824–825.

Jones F., Colfen H., and Antonietti M. (2000) Interaction of kappa-carrageenan with nickel cobalt and iron hydroxides. *Biomacromolecules* **1,** 556–563.

Kilcoyne S. H. and Lawrence J. L. (1999) The structure of iron dextran cores. *Z Kristallog.* **214,** 666–669.

Konhauser K. O. and Ferris F. G. (1996) Diversity of iron and silica precipitation by microbial mats in hydrothermal waters, Iceland: Implications for Precambrian iron formations. *Geology* **24,** 323–326.

Kroll E. and Winnik M. (1996) In situ preparation of nanocrystalline gamma-Fe$_2$O$_3$ in iron(II) cross-linked alginate gels. *Chem. Mater.* **8,** 1594–1597.

Kurimura Y. (1991) Multistep complexation of macromolecules. In *Macromolecular Complexes: Dynamic Interaction and Electronic Processes* (ed. E. Tsuchida), p. 13. VCH Verlagsgesellschaft.

Largeau C. (1995) Formation of Refractory Organic Matter from Biologic Precursors. In: The Role of Nonliving Organic Matter in The Earth's Carbon Cycle. R. G. Zepp, et al., eds, pp. 275–292. John Wiley and Sons Interscience.

Leppard G. G. (1995) The Characterization of algal and microbial mucilages and their aggregates in aquatic ecosystems. *Sci. Total Environ.* **165,** 103–131.

Leppard G. G. (1997) Colloidal organic fibrils of acid polysaccharides in surface waters: Electron-optical characteristics, activities and chemical estimates of abundance. *Colloids Surf. A* **120,** 1–15.

MacLachlan M. J., Manners I., and Ozin G. A. (2000) New (inter)faces. Polymers and inorganic materials. *Adv. Mater.* **12,** 675–684.

Mann S. (1993) Molecular tectonics in biomineralization and biomimetic materials chemistry. *Nature* **365,** 499–505.

McHale J. M., Auroux A., Perrotta A. J., and Navrotsky A. (1997) Surface energies and thermodynamic phase stability in nanocrystalline aluminas. *Science* **277,** 788–791.

Molyneux P. (1983) *Water-Soluble Synthetic Polymers: Properties and Behaviour,* Vol. 1. CRC Press.

Murray C. B., Kagan C. R., and Bawendi M. G. (2000) Synthesis and characterization of monodisperse nanocrystals and close-packed nanocrystal assemblies. *Ann. Rev. Mater. Sci.* **30,** 545–610.

Music S., Maljkovic M., and Popovic S. (1999) Chemical and microstructural properties of iron oxide powders obtained from FeCl$_3$ solutions with decomposing urea. *Ach-Models Chem.* **136,** 299–316.

Nesterova M., Walton S., and Webb J. (2000) Nanoscale iron(III) oxyhydroxy aggregates formed in the presence of functional water-soluble polymers: Models for iron(III) biomineralisation processes. *J. Inorg. Biochem.* **79,** 109–118.

Nyvlt J. (1995) The Ostwald rule of stages. *Cryst. Res. Technol.* **30,** 443–449.

Ohtaki M., Inata K., and Eguchi K. (1998) Selective incorporation of inorganic precursors into the channels of MCM-41 by molecular assembly template as a hydrophobic carrier. *Chem. Mater.* **10,** 2582–2584.

Ozin G. A., Hong Y., Sokolov I., and Coombs N. (1997) Shell mimetics. *Adv. Mater.* **9,** 662–667.

Penn R. L. and Banfield J. F. (1998a) Oriented attachment and growth twinning polytypism and formation of metastable phases: Insights from nanocrystalline TiO$_2$. *Am. Mineral.* **83,** 1077–1082.

Penn R. L. and Banfield J. F. (1998b) Imperfect oriented attachment: Dislocation generation in defect-free nanocrystals. *Science* **281,** 969–971.

Penn R. L., Oskam G., Strathmann G. J., Searson P. C., Stone A. T., and Veblen D. R. (2001) Epitaxial assembly in aged colloids. *J. Phys. Chem. B* **105,** 2177–2182.

Reeves N. J. and Mann S. (1991) Influence of inorganic and organic additives on the tailored synthesis of iron oxides. *J. Chem. Soc. Faraday Trans.* **87,** 3875–3880.

Saric A., Music S., and Nomura K. (1998) Influence of urotropin on the precipitation of iron oxides from FeCl3 solutions. *Croat. Chem. Acta* **71,** 1019–1036.

Schneider W., and Erni I. (1985) Chemistry of transit iron pools. In *Biochemistry and Physiology of Iron* (eds. P. Saltman et al.), pp. 121–145. Elsevier.

Schwertmann U., Friedl J., and Pfab G. (1996) A new iron(III) oxy-hydroxynitrate. *J. Solid State Chem.* **126,** 336.

Schwertmann U., Friedl J., Stanjek H., Murad E., and Bender Koch C. (1998) Iron oxides and smectites in sediments from Atlantis II Deep Red Sea. *Eur. J. Mineral.* **10,** 953–967.

Thomas-Keprta K. L., Clemett S. J., Bazylinski D. A., Kirschvink J. L., McKay D. S., Wentworth S. J., Vali H., Gibson E. K., McKay M. F., and Romanek C. S. (2001) Truncated hexa-octahedral magnetite crystals in ALH84001: Presumptive biosignatures. *Proc. Natl. Acad. Sci. USA* **98,** 2164–2169.

Williams R. L. P. (1984) An introduction to biominerals and the role of organic molecules in their formation. *Phil. Trans. R. Soc. Lond. B* **304,** 411–455.

Wirnsberger G., Gatterer K., Fritzer H. P., et al. (2001) Mesostructured iron oxyhydroxides. 1. Synthesis local structure and magnetism. *Chem. Mater.* **13,** 1453–1466.

Wu J., Boyle E., Sundra W., and Wen L-S. (2001) Soluble and colloidal iron in the oligotropic North Atlantic and North Pacific. *Science* **293,** 847–849.

Zhang H. Z. and Banfield J. F. (1998) A model for exploring particle size and temperature dependence of excess heat capacities of nanocrystalline substances. *Nanostruct. Mater.* **10,** 185–194.